Safety Analysis of Ranging Biases on the WAAS GEOs

Todd Walter, *Stanford University*
Juan Blanch, *Stanford University*
Eric Altshuler, *Sequoia Research Corporation*

Abstract

The Wide Area Augmentation System (WAAS) [1] has found that the ranging signals from its geostationary (GEO) satellites can significantly improve the availability of vertical guidance, particularly in Alaska and at times when not all GPS satellites are operational. However, WAAS has also observed that the GEO ranging sources can be affected by errors that are bias-like in their behavior [2] [3] [4] [5] [6] [7]. Such errors do not change values randomly but may persist with a particular sign and magnitude for many hours or longer. Some of these bias errors commonly affect our reference receivers and may thus be difficult to observe and bound in real time. Others are readily observable but not necessarily easy to eliminate as they may impact user receivers differently.

One such error results from incoherence between the code and the carrier signals. Unlike GPS, the GEO signals are generated on the ground and have to traverse the ionosphere both on the way up from the ground uplink station (GUS) to the GEO and then on the way down from the GEO to the user. The GUS electronics may not always be able to keep the two components perfectly aligned. This results in a code-carrier incoherency (CCI) that creates a varying error for users with different smoothing times. A user whose carrier smoothing filter has converged will see a different effect from a user who has not smoothed their code measurements with carrier data [2].

When WAAS generates a confidence bound on the ranging accuracy of the GEO satellites, it must account for all different users and for every error source. Unfortunately, the protection level equations used by WAAS do not support the inclusion of bias terms or terms to account for different smoothing times [8]. Therefore, WAAS must conduct special analyses to bound these biases. This paper describes the analysis WAAS performs to ensure that the UDRE it broadcasts for each GEO safely bounds all users for all possible bias errors. This analysis accounts for other fault modes that may also be present, but not yet detected by the WAAS integrity monitors.

Versions of GEO bias analyses have existed since before WAAS was commissioned in 2003. The analysis has been updated and significantly improved since those early more conservative approaches. WAAS is in the midst of replacing all three of its GEOs and will briefly have four operational ranging GEOs in the summer of 2019. Pseudorange bias terms can lead to much bigger user position errors when there are more such terms that may all align. This WAAS GEO bias analysis has been recently updated and each new GEO has been carefully examined to ensure the continued safe operation of GEO ranging. This paper describes this analysis and demonstrates the safety and performance of the new WAAS GEOs

Error Bounding Analysis

Because the broadcast sigmas (User Differential Range Error (UDRE) and Grid Ionospheric Vertical Error (GIVE)) are larger than the actual overbounds, constant biases up to a certain magnitude can be tolerated by the user. The analysis in this paper seeks to find the maximum tolerable biases that can be present for arbitrary geometries.

The analysis in this paper examines seven cases listed in Table 1. All seven cases must pass and each case itself has numerous subcases testing different UDREI and GIVEI values. Further the risk is evaluated against three user protection level calculations: the vertical and horizontal precision approach (PA) protection levels and the non-precision approach (NPA) horizontal protection level.

Table 1: GEO Bias Threat Cases from

Case Number	Description	Ionospheric State	Faulted SV
1	Fault-free Performance	Both Nominal and Storm	None
2	CCC Fault	Nominal-only	GPS
3	CCC Fault	Nominal-only	GEO
4	SQM Fault	Nominal-only	GPS
5	SQM Fault	Nominal-only	GEO
6	UDRE Fault	Nominal-only	GPS
7	UDRE Fault	Nominal-only	GEO

The fault cases evaluate whether faults will be safely detected even in the presence of the unfaulted GEO biases.

Probability of Position Error Exceeding the Protection Level

The purpose of the GEO Bias gaussian bounding analysis is to ensure that the broadcast UDRE and GIVE values are at least as large enough to bound the user's actual errors. This can be written mathematically as:

$$K_{MOPS}\sqrt{\sum_{i=1}^{N} s_{x,i}^2\sigma_{B,i}^2} \geq K_{PE>PL+}\sqrt{\sum_{i=1}^{N} s_{x,i}^2\sigma_{a,i}^2} + \sum_{i=1}^{N}\left|s_{x,i}\mu_i\right| \quad (1)$$

where the left side is the user computed Protection Level (PL) and the right side is a conservative representation of the actual position error assuming a Gaussian overbounding model. K_{MOPS} is the WAAS Minimum Operational Performance Standards (MOPS) [8] Gaussian K-factor corresponding to the PL (e.g. 5.33 for vertical), $s_{x,i}$ is the projection from the i^{th} satellite range measurement to the user position error in the *x* direction, $\sigma_{B,i}$ is the broadcast sigma (which is derived from the UDRE and GIVE values), $K_{PE>PL+}$ the Gaussian K-factor that corresponds to the desired probability bound on the position error exceeding the protection level for the right tail, $\sigma_{a,i}$ is the actual overbounding sigma for the data, and μ_i is the actual bias overbound. The equation calculates the one-sided probability of the position error exceeding the protection level. There is also a small contribution from the left Gaussian tail (in the

direction opposite the bias terms) that will be considered later. We can solve for the maximum $K_{PE>PL}$ supported given the broadcast sigmas and the actual sigmas and biases:

$$K_{PE>PL+} = \frac{K_{MOPS}\sqrt{\sum_{i=1}^{N} s_{x,i}^2 \sigma_{B,i}^2} - \sum_{i=1}^{N} \left| s_{x,i}\mu_i \right|}{\sqrt{\sum_{i=1}^{N} s_{x,i}^2 \sigma_{a,i}^2}} \tag{2}$$

The first order probability of the position error exceeding the protection level can be obtained, for example, through the Matlab function normcdf: $P_{PE>PL}$ = normcdf(-$K_{PE>PL+}$) [9]. Unfortunately, (2) depends upon the user's geometry through the $s_{x,i}$ terms. In this section, we will provide a simplified solution, but the actual evaluation uses the optimal solution presented in the appendix of this paper. First, we define the ratio $\alpha_i = \frac{\sigma_{B,i}}{\sigma_{a,i}}$. If we further define $\alpha_{\min} = \min_i \frac{\sigma_{B,i}}{\sigma_{a,i}}$, we can bound the middle term of (1):

$$\sqrt{\sum_{i=1}^{N} s_{x,i}^2 \sigma_{a,i}^2} \le \frac{1}{\alpha_{\min}} \sqrt{\sum_{i=1}^{N} s_{x,i}^2 \sigma_{B,i}^2} \tag{3}$$

Using the Cauchy-Schwartz inequality we can bound the last term of (1):

$$\sum_{i=1}^{N} \left| s_{x,i}\sigma_{B,i} \times \frac{\mu_i}{\sigma_{B,i}} \right| \le \sqrt{\sum_{i=1}^{N} s_{x,i}^2 \sigma_{B,i}^2} \times \sqrt{\sum_{i=1}^{N} \frac{\mu_i^2}{\sigma_{B,i}^2}} \tag{4}$$

Therefore, we can rewrite the requirement in (1) as:

$$K_{MOPS}\sqrt{\sum_{i=1}^{N} s_{x,i}^2 \sigma_{B,i}^2} \ge \frac{K_{PE>PL+}}{\alpha_{\min}} \sqrt{\sum_{i=1}^{N} s_{x,i}^2 \sigma_{B,i}^2} + \sqrt{\sum_{i=1}^{N} s_{x,i}^2 \sigma_{B,i}^2} \times \sqrt{\sum_{i=1}^{N} \frac{\mu_i^2}{\sigma_{B,i}^2}} \tag{5}$$

which can be simplified to:

$$K_{MOPS} \ge \frac{K_{PE>PL+}}{\alpha_{\min}} + \sqrt{\sum_{i=1}^{N} \frac{\mu_i^2}{\sigma_{B,i}^2}} \tag{6}$$

We now have a form of (1) that does not depend upon user geometry. We can again rearrange the equation to determine the probability of violating the PL given a set of biases and $\alpha_{\min}$:

$$P_{PE>PL+} = \text{normcdf}\left(-\alpha_{\min}\left[K_{V,PA} - \sqrt{\sum_{i=1}^{N}\frac{\mu_i^2}{\sigma_{B,i}^2}}\right]\right) \tag{7}$$

Because geometry is not part of this equation, the risk of exceeding either the precision approach vertical or horizontal protection levels can be calculated simply by replacing K_{MOPS} with $K_{V,PA}$ or $K_{H,PA}$ respectively while the risk of exceeding the non-precision approach horizontal protection level is given by replacing K_{MOPS} with $K_{H,NPA}$. This simplified formula requires the use of the minimum α over all satellites. A better solution is derived in the appendix that provides the probability using individual α_i terms and that accounts for the left tail contribution to the probability. This optimal calculation finds a smaller probability than (7) and is used by the later analysis of the WAAS GEO biases. The probability given in the appendix by (A.21) only depends upon K_{MOPS}, α_i, and $\gamma_i = \frac{\mu_i}{\sigma_{a,i}}$.

Determination of σ_B, σ_a, μ, α, and γ

The analysis begins by calculating $\sigma_{B,i}$, $\sigma_{a,i}$, μ_i, α, and γ values for the GPS satellites and GEO satellites under both nominal and storm ionospheric conditions. It does this by first calculating $\sigma_{B,i}$, $\sigma_{a,i}$, and μ_i for each condition, for each possible UDRE index (UDREI) and each GIVE index (GIVEI) values. For GPS, these are given by:

$$\sigma_{B,i}^2(UDREI, GIVEI, el) = \sigma_{flt}^2(UDREI) + \sigma_{UIRE}^2(GIVEI, el) + \sigma_{trop}^2(el) + \sigma_{air}^2(el) \tag{8}$$

$$\begin{aligned}\sigma_{a,i}^2(UDREI, GIVEI, el) = {} & \sigma_{flt}^2(UDREI)\times\sigma_{ob,UDRE}^2(UDREI) + \\ & \sigma_{UIRE}^2(GIVEI, el)\times\sigma_{ob,UIVE}^2(GIVEI) + \\ & \sigma_{trop}^2(el)\times\sigma_{ob,trop,vert}^2 + \sigma_{air}^2(el)\times\sigma_{ob,air}^2\end{aligned} \tag{9}$$

$$\begin{aligned}\mu_i(UDREI, GIVEI, el) = {} & \sigma_{flt}(UDREI)\times\mu_{ob,UDRE}(UDREI) + \\ & \sigma_{UIRE}(GIVEI, el)\times\mu_{ob,UIVE}(GIVEI) + \\ & \sigma_{trop}(el)\times\mu_{ob,trop,vert} + \sigma_{air}(el)\times\mu_{ob,air} + Bias_{nom}\end{aligned} \tag{10}$$

Where $\sigma_{flt} = \sigma_{UDRE} \times \delta UDRE$, σ_{UIRE} is the interpolated value of σ_{GIVE} at the user pierce point location multiplied by the obliquity factor, σ_{trop} is the tropospheric overbound from the SBAS MOPS [8], σ_{air} is the airborne receiver noise and multipath overbound also from the SBAS MOPS [8] and $Bias_{nom}$ is an assumed nominal bias term. Note that for GPS $\delta UDRE$ is conservatively set to 1. The σ_{ob} terms are the empirical normalized overbounds for each term and the μ_{ob} terms are the sample means overbounding values. As an example, Table 2 shows the input sigma values from our GEO and GPS UDRE overbounding analysis. Means and normalized overbounding sigma values are calculated for the all GPS satellites as well as each GEO and at each UDREI value. Values are normalized by σ_{UDRE} so any value less than 1 in the table is considered an overbound. The small ratios (all below 0.35) indicates that there is a lot of margin to exploit for covering the biases.

Table 2: GEO & GPS Normalized Overbounding Sigmas by UDREI

Satellite	UDREI	N_{points}	Mean	σ_{OBMC}
CRW (135)	10	112682	0.0007	0.281
	11	4453	-0055	0.129
CRE (138)	10	116779	0.0006	0.244
	11	3569	-0.0103	0.087
SM9 (131)	10	116079	-0.0035	0.214
	11	9596	0.0220	0.056
S15 (133)	10	108909	-0.0034	0.237
	11	8120	0.0230	0.109
GPS (1 -32)	5	867766	0.0083	0.232
	6	205648	-0.0171	0.208
	7	98013	-0.0099	0.207
	8	44964	-0.0111	0.194
	9	20964	-0.0110	0.190
	10	15240	-0.0163	0.255
	11	13186	-0.0122	0.114
	12	3973	-0.0044	0.031
	13	55	-	-

The probability in (A.21) is evaluated at all elevation angles for the GPS data between 5 and 90 degrees for each UDREI and GIVEI. The arguments that lead to the largest probability are used to record α_i, and γ_i for both the nominal and storm ionospheric conditions.

For the GEOs, similar calculations are made, except that the operational static MT28 values are used to evaluate the actual $\delta UDRE$. The equations for $\sigma_{B,i}$, $\sigma_{a,i}$, and μ_i are evaluated throughout the GEO footprint from 15 to 75 degrees North, and from 170 to 55 degrees West, at one degree increments. The analysis finds the α_i and γ_i values corresponding to maximum probability of exceeding the PL across all UDREIs, GIVEIs and user locations.

Figure 1 shows the σ_B values over this region for PRN 131 with a UDRE of 7.5 m and GIVE values of 3 m everywhere. This is a conservative estimate as it includes lines-of-sight outside of the broadcast ionospheric grid and below the line where all GIVEs are set to 15 m or above. Values for σ_B, σ_a, μ, $\alpha < \sigma_a/\sigma_B$, $\gamma < \mu/\sigma_B$, and $K_{PE>PL+}$, were calculated at each location (SM9 was the 3rd GEO entered into the analysis hence GEO #3 in the title). The maximum α and μ values and the minimum $K_{PE>PL+}$ values shown in the title are used for later computation.

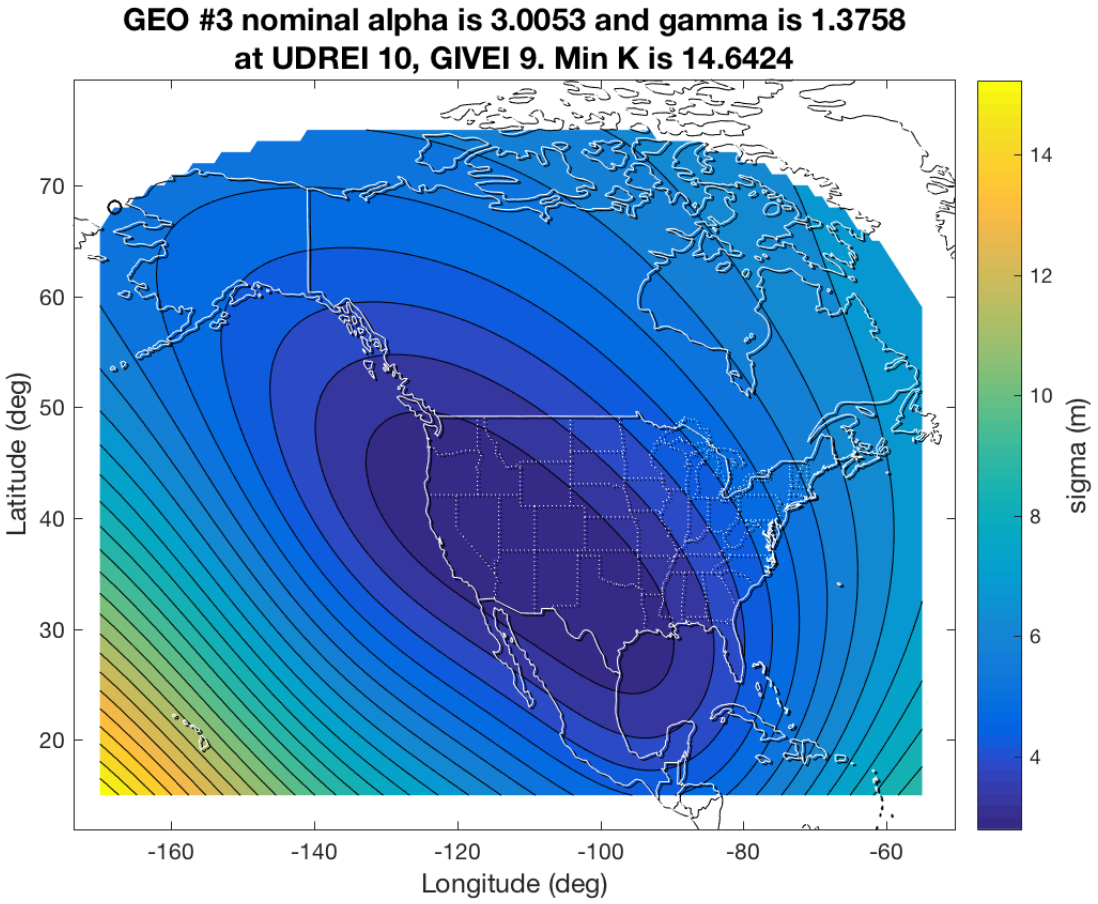

Figure 1. The SM9 Values of σ_B as a Function of User Location.

Unfaulted Probability

Next in the calculation we consider four vectors each with n_{GPS} identical elements and n_{GEO} elements. The latter are each unique to its GEO. One pair of vectors contains the worst-case α and γ values for nominal ionospheric conditions, and the other pair, their corresponding values for storm conditions. These vectors are sufficient to determine the probability of exceeding the protection levels for fault-free conditions. The optimal probability in (A.21) is evaluated and the probabilities for nominal and storm conditions are each compared against their specific integrity allocation for both the horizontal and vertical nodes. Generally, the storm ionospheric conditions are expected to have less margin and

therefore a larger overall P_{HMI}. The analysis considers that this particular evaluation passes if the vertical $P_{VPE>VPL}$ and the horizontal $P_{HPE>HPL}$ are below their respective fault-free allocations.

The fault-free results are shown in Table 3 below. The analysis outputs the maximum between iono storm and non-storm conditions with the storm conditions always being worse. As can be seen there is substantial margin between the nominal risk and the allocated risk for all three evaluated operations.

Table 3: Nominal GEO bias integrity risk

	Vertical PA	Horizontal PA	Horizontal NPA
Storm	4.63×10^{-16} /approach	2.90×10^{-20} /approach	4.21×10^{-20} /hour
Allocation	6.66×10^{-10}/approach	3.33×10^{-10}/approach	1.00×10^{-9}/hour

The next sections analyze the influence of the biases when a fault is present. For the remainder of the evaluations only the nominal ionospheric conditions are considered. It is considered sufficiently unlikely that a fault onset will occur in the narrow window of time when a severe ionospheric storm is beginning, but the ionospheric storm detectors have not yet tripped.

CCC Faults

In the faulted cases, only the nominal ionospheric α and γ values are used. For one satellite, the nominal values are replaced with values corresponding to specific fault scenarios. Threats are evaluated for each UDREI and GIVEI. Beginning with GPS, a bias is added to the bounding nominal μ_i value. This bias is evaluated in from 0 to many times the value for the UDREI. A new γ is calculated according to

$$\gamma_{GPS,fault}(UDREI, GIVEI, b_{fault}) = \frac{\mu_{GPS,nom}(UDREI, GIVEI) + b_{fault}}{\sigma_{a,GPS,nom}(UDREI, GIVEI)} \tag{11}$$

And a corresponding α is calculated

$$\alpha_{GPS,fault}(UDREI, GIVEI) = \frac{\sigma_{B,GPS,nom}(UDREI, GIVEI)}{\sigma_{a,GPS,nom}(UDREI, GIVEI)} \tag{12}$$

These values replace one of the nominal GPS values in the nominal ionospheric α and γ vectors and are then used to evaluate $P_{PE>PL}$(*UDREI*, *GIVEI*, b_{fault}) using (A.21).

The analysis also calculates the probability of missed detection, P_{md}, for the CCC monitor given a fault of magnitude b_{fault}. This is obtained from the CCC monitor threshold, T_{CCC}(*UDREI*) and the CCC monitor test statistic σ_{test}(*UDREI*):

$$P_{md,CCC}(UDREI, b_{fault}) = \text{normcdf}\left(-\frac{b_{fault} - T_{CCC}(UDREI)}{\sigma_{test}(UDREI)}\right) \tag{13}$$

The CCC metric values used by the analysis are listed in Table 4. The values are listed in meters. The maximum value is applied to all GEOs and to all larger UDREI values.

Table 4: GEO CCC Metric values in meters

	CRW	**CRE**	**SM9**	**S15**	**Final**
UDREI	$\sigma_{test,L1}$	$\sigma_{test,L1}$	$\sigma_{test,L1}$	$\sigma_{test,L1}$	$\sigma_{CCC,GEO}$
10	0.502	0.434	0.643	0.409	0.643
11	0.155	0.344	0.198	0.150	0.643

Finally, an *a priori* rate of CCC fault is also applied. The final calculation of HMI for a CCC fault is then the maximum value of the product of these three probabilities:

$$P_{CCC} = \max_{UDREI,GIVEI,b_{fault}} P_{a\ priori,CCC} \times P_{md,CCC}\left(UDREI, b_{fault}\right) \times P_{PE>PL,CCC}\left(UDREI,, GIVEI, b_{fault}\right) \quad (14)$$

Figure 2 illustrates this process as a function of the CCC fault magnitude. The red lines show the probability that the actual user error will exceed the corresponding protection level for the provided sigmas and biases including the fault bias whose magnitude is shown on the x-axis. There are three lines with the solid line corresponding to the Vertical Protection Level (VPL), the dashed line corresponding to the matching Horizontal Protection Level (HPL), and the dashed dot line corresponding to the HPL for Non-Precision Approach (NPA). As expected, these lines increase as the fault magnitude increases and gradually approach one as the fault magnitude exceeds the UDRE (7.5 m in this example). The blue line shows the probability that the CCC monitor will fail to detect a fault of such magnitude. It starts at 1 for very small faults and goes to 50% at the monitor threshold (around 5 m for this UDREI) and rapidly becomes smaller as the magnitude increases. The cyan lines show the prior probability that CCC fault will be present during the period of time of the operation (150 seconds for vertical or LPV and one hour for NPA). The magenta lines show the product of these three lines and shows the probability that a fault will be present, will go undetected, and lead to a Position Error (PE) that exceeds the PL. It is evaluated as a function of the fault magnitude and the maximum value is selected.

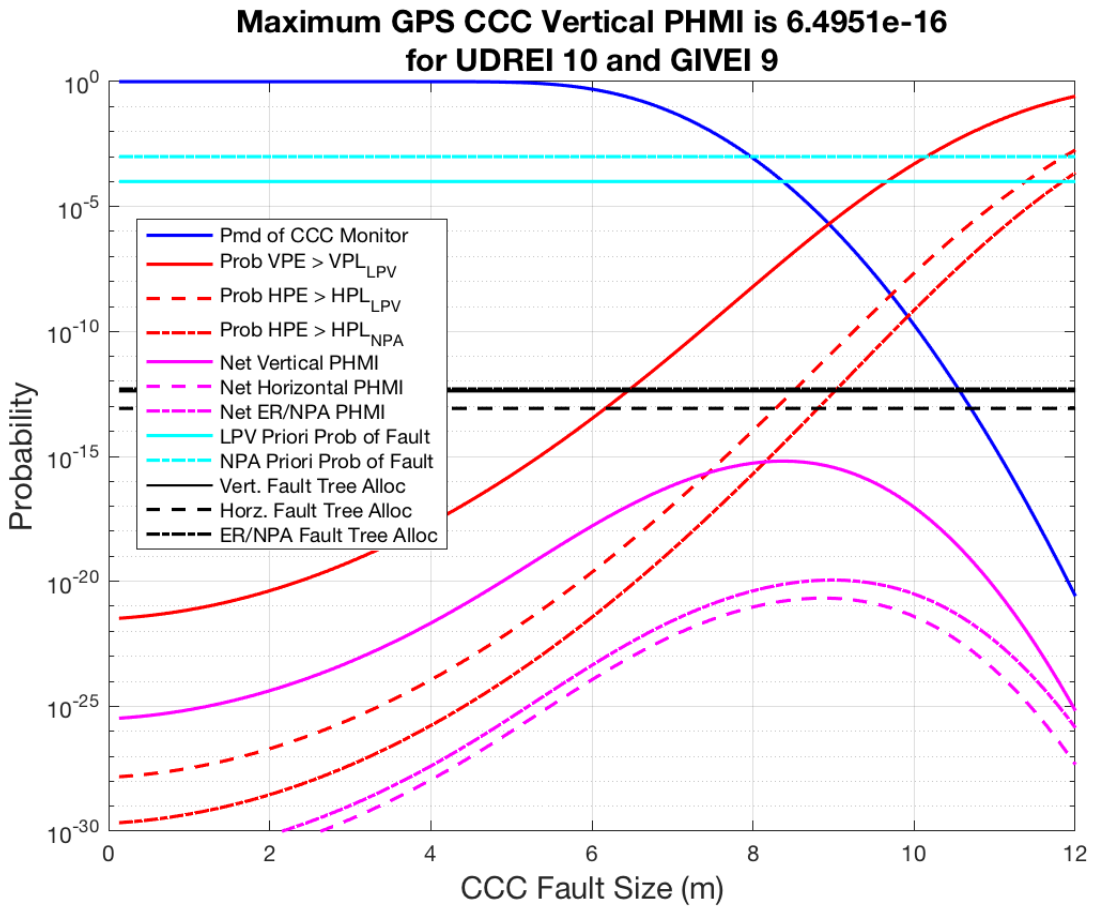

Figure 2 GPS CCC Fault Probabilities

The black lines represent the WAAS fault tree allocation for a CCC fault creating Hazardously Misleading Information (HMI) on a GPS satellite for each operation. As can be seen, the magenta line is below the black line for all possible fault values. This value was evaluated for all possible values of UDREI and GIVEI and the risk was maximized for the values of UDREI = 10 and GIVEI = 9 as shown in the plot.

The same process is used then applied to each GEO in turn. The only difference is that because the nominal GEO bias is predominantly caused by code-carrier incoherence that the monitor is designed to detect, the faulted bias replaces the nominal bias, unlike the GPS case and all subsequent GEO fault cases. Figure 3 shows these results where the maximum also occurred for UDREI = 10 and GIVEI = 9 and on PRN 131. Note that for the GEO CCC fault the prior probability of fault is considered to be 1. Again the probabilities meet their respective allocations.

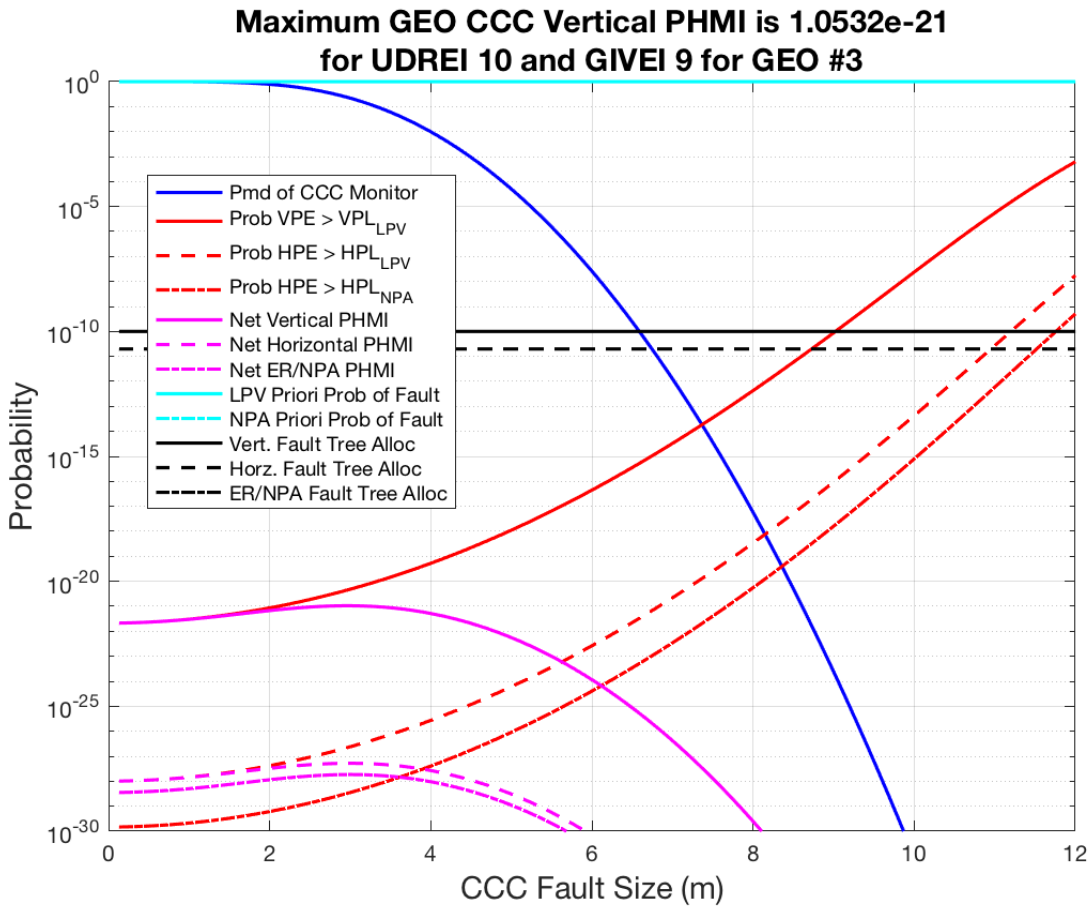

Figure 3 GEO CCC Fault Probabilities on PRN 131

SQM Faults

A similar process is used to evaluate SQM faults as is described in the previous section. It is also more difficult to evaluate P_{md} in the user range domain for the SQM Monitor. An SQM analysis evaluates the ability of the monitor to detect values in the SQM metric domain. It then maps these values through the SQM fault model to determine the corresponding maximum user threat. These biases and P_{md} values are then tabulated and recorded for use for this GEO bias analysis. The biases are used to create faulted α and γ elements that are calculated as in (11) and (12). Additionally, an *a priori* is used:

$$P_{SQM} = \max_{UDREI,GIVEI,b_{fault}} P_{a\ priori,SQM} \times P_{md,SQM}\left(UDREI, b_{fault}\right) \times P_{PE>PL,SQM}\left(UDREI,, GIVEI, b_{fault}\right) \quad (15)$$

This maximum is calculated for both the vertical and horizontal case and then compared to the corresponding SQM GPS fault tree allocation. The same process is applied to each GEO in turn. Figure 4 shows the worst-case result for the GPS SQM threat analysis.

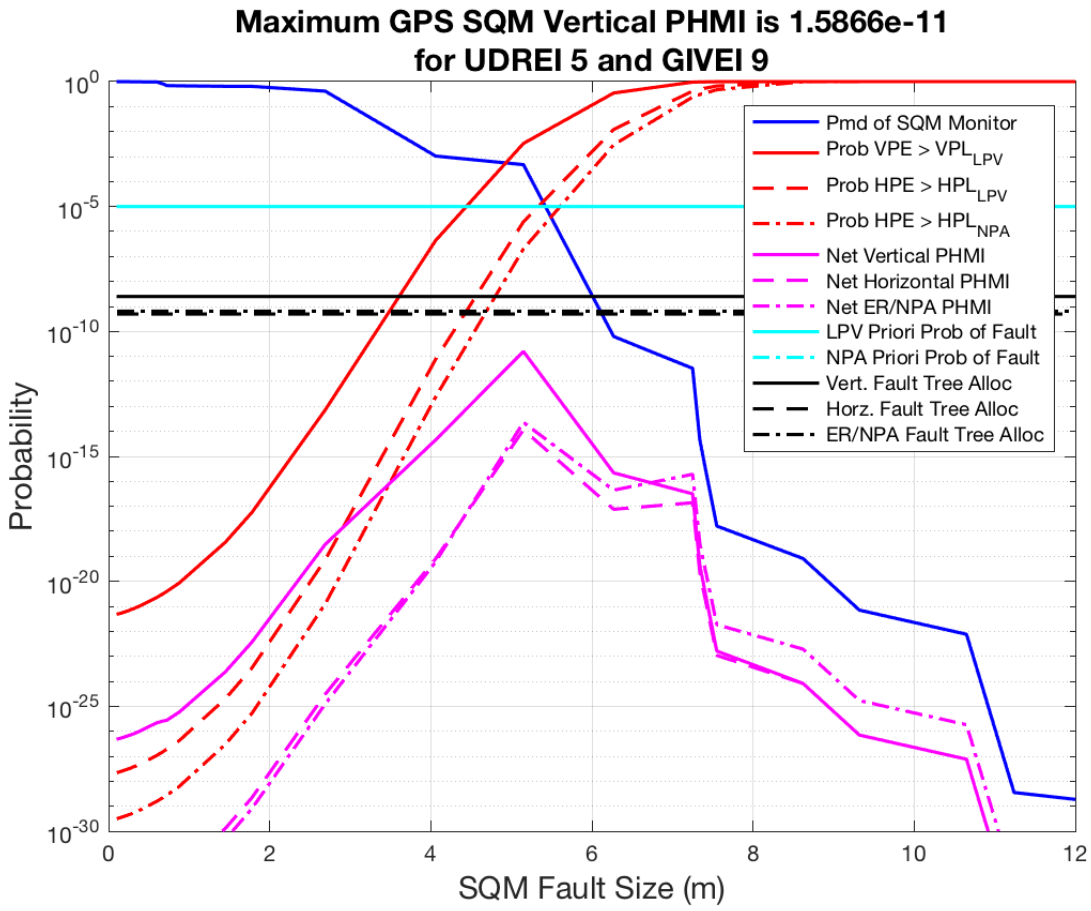

Figure 4 GPS SQM Fault Probabilities

UDRE Faults

The UDRE fault evaluation is similar to the SQM fault evaluation. However, unlike the CCC and SQM monitors, the UDRE monitor does not have a unique P_{md} given a bias and a UDREI. Instead, there are a range of possible P_{md} values that depend upon the number and quality of the reference station observations. A simulation was run using our Matlab Algorithm Availability Simulation Toolset (MAAST) [10] with the standard constellation specified in Appendix B of the WAAS MOPS [8]. Every five minutes, over a 24-hour period, the UDRE monitor equations were evaluated for each satellite in view. A range of biases were evaluated from zero to the MERR value, to determine the corresponding $P_{md}(UDREI, b_{fault})$ for that specific observing geometry. The maximum P_{md} for each *UDREI* and b_{fault} were determined across all satellites and all time-steps. This maximum P_{md} and the corresponding biases were recorded into files for use in the analysis. For the *a priori* probability, a conservative value of 1 is used. The net PHMI for the faulted UDRE case is then the product of the three probabilities:

$$P_{UDRE} = \max_{UDREI,GIVEI,b_{fault}} P_{a\ priori,UDRE}\left(UDREI,b_{fault}\right)\times P_{md,\max,UDRE}\left(UDREI,b_{fault}\right) \times P_{PE>PL,UDRE}\left(UDREI,,GIVEI,b_{fault}\right) \quad (16)$$

This maximum is calculated for both the vertical and horizontal cases and then compared to the corresponding UDRE GPS fault tree allocations. The same process is applied to each GEO in turn. Figure 5 shows the worst-case results of the GPS UDRE evaluation.

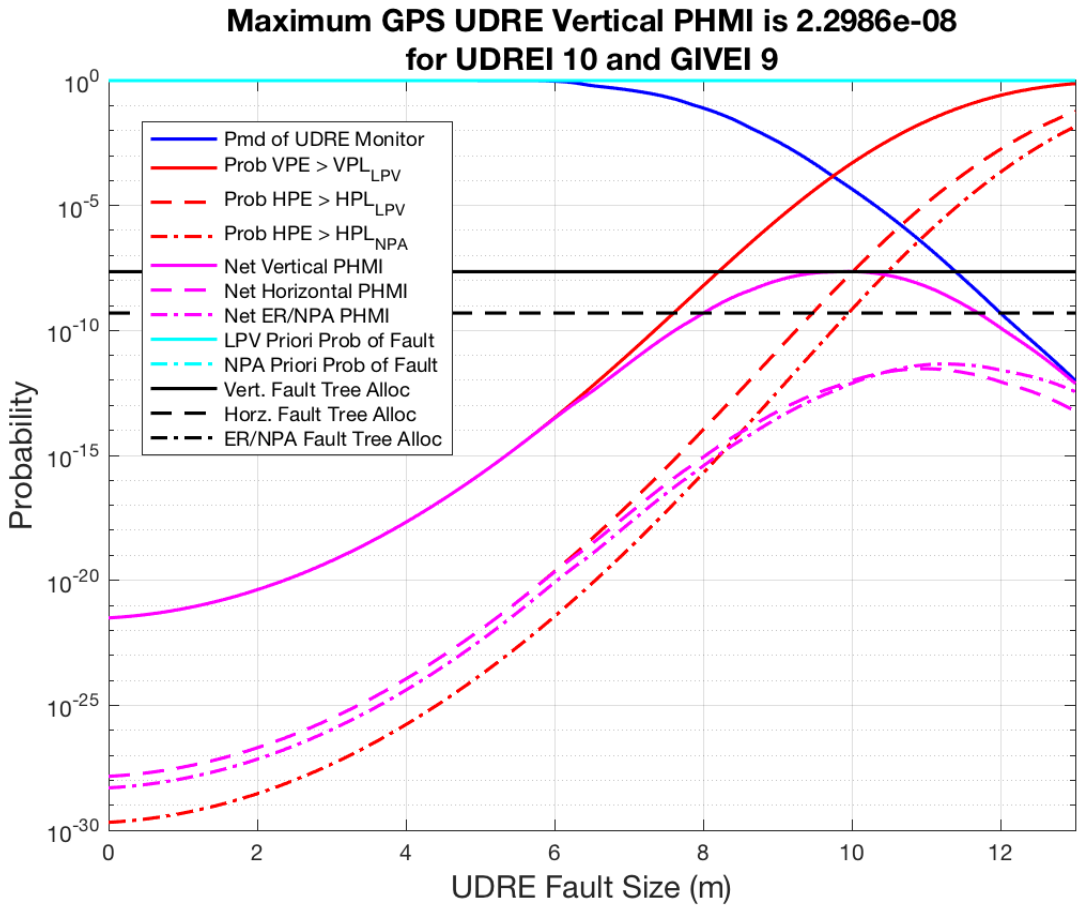

Figure 5 GPS UDRE Fault Probabilities

Summary of Results

Table 5 shows the summary results for all 7 cases. Nearly all of the above evaluations meet their allocations and therefore successfully pass. The one failure case is for a GPS UDRE fault with a UDREI value of 10 and a GIVEI value of 9 as shown in Figure 5. This indicates that there could be an excess risk of 5×10^{-10} due to this underbounding. However, this analysis is extremely conservative and assumes that all sigma values are at their minimum values and all biases are at their maximum value and aligned with the worst possible combination of signs. Given these conservative assumptions, It is likely that the calculation itself is overly conservative by at least this margin. Further, it can be seen that some of the other fault cases pass with more margin than this. Thus, it is possible to reallocate risk on the fault tree and meet our top level objective. Therefore, it is recommended that the system can operate with all four GEOs for several weeks and still meet its integrity requirements.

Table 5: Largest Risk Per Case

Fault-free Performance	None	6.66×10^{-10}	4.63×10^{-16}
CCC Fault	GPS	4.17×10^{-13}	6.50×10^{-16}
CCC Fault	GEO	1.00×10^{-10}	1.05×10^{-21}
SQM Fault	GPS	2.50×10^{-9}	1.59×10^{-11}
SQM Fault	GEO	2.50×10^{-9}	1.67×10^{-9}
UDRE Fault	GPS	2.25×10^{-8}	**2.30×10^{-8} (1.47×10^{-8} for 3 GEOS)**
UDRE Fault	GEO	2.25×10^{-8}	1.30×10^{-8}

The analysis also examined the case where CRW is retired and only three GEOs are operating, the expected long-term operational case. It found that when there are only three GEOs all of the above numbers decrease, and the GPS UDRE fault case goes below its allocation. It will now have the value of 1.47×10^{-8}. This analysis has demonstrated that the observed system performance allows the maximum 2.5 m GEO CMCI biases tolerated by the CCC monitor trip thresholds to be present on all three GEOs and still meet the overall PHMI requirements. It further argues that temporary or even extended operation with four GEOs is safe given the extremely conservative nature of the analysis. This section demonstrates that sufficient margin exists to handle both the fault-free and faulted conditions.

Conclusions

The GEO bias analysis examines the risk of unbounded position errors due to the simultaneous presence of nominal bias terms (>2.5 m in the case of the GEOs) and faults. The analysis demonstrates that the combination of the prior probability of the fault occurrence, the probability that the monitors will fail to detect the fault, and the probability that the position error will exceed the corresponding protection level is smaller that the allocated probability of hazardously misleading information (HMI) in the WAAS fault tree with one exception. That exception is sufficiently close to the requirement, that the excess risk can be absorbed by other sections of the fault tree. Therefore the conclusion of the analysis is that the proposed operation meets the top level safety requirement. The analysis utilizes the large margin between the broadcast confidence bounds (UDRE and GIVE) and the actual error distribution Gaussian overbounds. There are several conservative steps in the process that allow it to be applied for every geometry and for worst possible combinations of biases, faults, and nominal errors. The appendix derives a method to apply separate upper bounds (i.e. the α_{min} parameter) for each of the GEOS and for all of the GPS satellites. This new method allows for a significant reduction in the upper bound of the estimated probability of HMI (PHMI). Using this approach, we have been able to validate that despite the potential presence of large biases on each GEO, the GEO UDRE values could be set as low as 7.5 m on WAAS for the proposed four operational GEOs. Previous analyses could not support such large

biases on multiple GEOs. This analysis allows WAAS to retain useful range error bounds on all four of its GEOs and increase vertical guidance availability of the system.

References

[1] Walter, Todd, Shallberg, Karl, Altshuler, Eric, Wanner, William, Harris, Chris, Stimmler, Robert, "WAAS at 15," *Proceedings of the 2018 International Technical Meeting of The Institute of Navigation*, Reston, Virginia, January 2018, pp. 301-321.

[2] Cheung, Laura, Hsu, Po-Hsin, "WAAS Single Frequency GEO Operation Field Test and L1 Signal Code-Carrier Coherence Results," Proceedings of the 24th International Technical Meeting of The Satellite Division of the Institute of Navigation (ION GNSS 2011), Portland, OR, September 2011, pp. 2446-2452.

[3] Shallberg, Karl, Grabowski, Joe, "Considerations for Characterizing Antenna Induced Range Errors," *Proceedings of the 15th International Technical Meeting of the Satellite Division of The Institute of Navigation (ION GPS 2002)*, Portland, OR, September 2002, pp. 809-815.

[4] Phelts, R. Eric, Walter, Todd, Enge, Per, Akos, Dennis M., Shallberg, Karl, Morrissey, Tom, "Range Biases on the WAAS Geostationary Satellites," *Proceedings of the 2004 National Technical Meeting of The Institute of Navigation*, San Diego, CA, January 2004, pp. 110-120.

[5] Shallberg, Karl W., Ericson, Swen D., Phelts, Eric, Walter, Todd, Kovach, Karl, Altshuler, Eric, "Catalog and Description of GPS and WAAS L1 C/A Signal Deformation Events," Proceedings of the 2017 International Technical Meeting of The Institute of Navigation, Monterey, California, January 2017, pp. 508-520.

[6] Shallberg, Karl, Sheng, Fang, "WAAS Measurement Processing; Current Design and Potential Improvements," *Proceedings of IEEE/ION PLANS 2008*, Monterey, CA, May 2008, pp. 253-262.

[7] Shallberg, Karl, Potter, B.J., Class, Phillip, "Geostationary Satellite Reference Station Multipath Characterization: Using Galaxy 15 Failure to Refine the WAAS Multipath Threat," *Proceedings of the 24th International Technical Meeting of The Satellite Division of the Institute of Navigation (ION GNSS 2011)*, Portland, OR, September 2011, pp. 2453-2461.

[8] RTCA, "Minimum Operational Performance Standards for Global Positioning System/ Satellite-Based Augmentation System Airborne Equipment," DO-229E, December, 2016.

[9] http://www.mathworks.com

[10] Jan, S., Chan, W., and Walter, T., "MATLAB Algorithm Availability Simulation Tool," Published in GPS Solutions, Vol. 13., No. 4, September 2009.

Appendix Derivation of Optimal Calculation

The optimal evaluation of (2) can be computed by finding the minimum value over all possible geometries:

$$\min_{s_{x,i}} \left(\frac{K_{MOPS} \sqrt{\sum_{i=1}^{N} s_{x,i}^2 \sigma_{B,i}^2} - \sum_{i=1}^{N} \left| s_{x,i} \mu_i \right|}{\sqrt{\sum_{i=1}^{N} s_{x,i}^2 \sigma_{a,i}^2}} \right) \tag{A.1}$$

This can be solved with Lagrange multipliers as follows:

$$x_i = \frac{s_{x,i} \sigma_{a,i}}{\sqrt{\sum_{i=1}^{N} s_{x,i}^2 \sigma_{a,i}^2}} \tag{A.2}$$

The problem becomes:

$$\min_{\substack{x^T x=1 \\ x_i \geq 0}} \left(K_{MOPS} \sqrt{\sum_{i=1}^{N} x_i^2 \frac{\sigma_{B,i}^2}{\sigma_{a,i}^2}} - \sum_{i=1}^{N} x_i \frac{\mu_i}{\sigma_{a,i}} \right) = \min_{\substack{x^T x=1 \\ x_i \geq 0}} \left(K_{MOPS} \sqrt{\sum_{i=1}^{N} x_i^2 \alpha_i^2} - \sum_{i=1}^{N} x_i \gamma_i \right) \tag{A.3}$$

Where we have substituted α and γ as defined in the previous sections. We define the Lagrangian associated to this problem:

$$L(x, \lambda) = K_{MOPS} \sqrt{\sum_{i=1}^{N} x_i^2 \alpha_i^2} - \sum_{i=1}^{N} x_i \gamma_i + \frac{\lambda}{2} \left(x^T x - 1 \right) \tag{A.4}$$

Because we want to find the minimum with respect to *x*, we calculate the derivative:

$$\frac{\partial L}{\partial x_j}(x, \lambda) = K_{MOPS} \frac{x_j \alpha_j^2}{\sqrt{\sum_{i=1}^{N} x_i^2 \alpha_i^2}} - \gamma_j + \lambda x_j \tag{A.5}$$

The minimum will occur at $\frac{\partial L}{\partial x_j}(x, \lambda) = 0$, from which we obtain:

$$x_j\left(K_{MOPS}\frac{\alpha_j^2}{\sqrt{\sum_{i=1}^{N}x_i^2\alpha_i^2}}+\lambda\right)=\gamma_j \tag{A.6}$$

We can separate *x* and square both sides to obtain

$$x_j^2=\frac{\gamma_j^2\sum_{i=1}^{N}x_i^2\alpha_i^2}{\left(K_{MOPS}\alpha_j^2+\lambda\sqrt{\sum_{i=1}^{N}x_i^2\alpha_i^2}\right)^2} \tag{A.7}$$

We can cancel the *x* terms on the left side and the numerator of the right by multiplying by α_j^2 and summing over *j*.

$$\sum_{j=1}^{N}x_j^2\alpha_j^2=\sum_{j=1}^{N}\frac{\alpha_j^2\gamma_j^2\sum_{i=1}^{N}x_i^2\alpha_i^2}{\left(K_{MOPS}\alpha_j^2+\lambda\sqrt{\sum_{i=1}^{N}x_i^2\alpha_i^2}\right)^2} \tag{A.8}$$

Cancellation yields

$$1=\sum_{j=1}^{N}\frac{\alpha_j^2\gamma_j^2}{\left(K_{MOPS}\alpha_j^2+\lambda\sqrt{\sum_{i=1}^{N}x_i^2\alpha_i^2}\right)^2} \tag{A.9}$$

We then define a new variable ϕ:

$$\phi=\lambda\sqrt{\sum_{i=1}^{N}x_i^2\alpha_i^2} \tag{A.10}$$

So that we now only need to solve a function with the single variable ϕ whose optimal values satisfies:

$$1=\sum_{j=1}^{N}\frac{\alpha_j^2\gamma_j^2}{\left(K_{MOPS}\alpha_j^2+\phi_{opt}\right)^2} \tag{A.11}$$

Because both x_j and γ_j are greater than or equal to zero, we know that the quantity inside the parentheses in (A.6) must also be greater than or equal to zero. This requirement is equivalent to:

$$K_{MOPS}\alpha_j^2 + \phi \geq 0 \tag{A.12}$$

We also know that the optimal value of ϕ minimizes (A.11), so that:

$$\sum_{j=1}^{N} \frac{\alpha_j^2 \gamma_j^2}{\left(K_{MOPS}\alpha_j^2 + \phi\right)^2} \leq 1 \tag{A.13}$$

Therefore:

$$\alpha_j \gamma_j - K_{MOPS}\alpha_j^2 \leq \phi_{opt} \tag{A.13}$$

The search for ϕ_{opt} can be done numerically by interval halving starting between upper and lower values:

$$\begin{aligned} \phi_{lower} &= \max_j\left(\alpha_j \gamma_j - K_{MOPS}\alpha_j^2\right) \\ \phi_{upper} &= \max_j\left(\alpha_j \gamma_j \sqrt{N+1} - K_{MOPS}\alpha_j^2\right) \end{aligned} \tag{A.14}$$

The analysis evaluates the midpoint in (A.13) and if result of the sum is greater than one, the midpoint becomes the new upper bound. Otherwise the midpoint becomes the new lower bound. The process is repeated until the difference between the upper and lower bounds is below a threshold (set to 10^{-7}). Once ϕ_{opt} is determined, we determine λ by putting (A.10) into (A.7):

$$x_j^2 = \frac{\gamma_j^2 \frac{\phi_{opt}^2}{\lambda^2}}{\left(K_{MOPS}\alpha_j^2 + \phi_{opt}^2\right)^2} \tag{A.15}$$

Applying the constraint

$$\sum_{j=1}^{N} x_j^2 = 1 \tag{A.16}$$

We can solve for λ:

$$\lambda = \sqrt{\sum_{j=1}^{N} \frac{\gamma_j^2 \phi_{opt}^2}{\left(K_{MOPS}\alpha_j^2 + \phi_{opt}^2\right)^2}} \tag{A.17}$$

We can then use (A.15) to solve for x_j:

$$x_{j,opt} = \frac{\gamma_j}{\left(K_{MOPS}\alpha_j^2 + \phi_{opt}^2\right)\sqrt{\sum_{i=1}^{N} \frac{\gamma_i^2}{\left(K_{MOPS}\alpha_i^2 + \phi_{opt}^2\right)^2}}} \tag{A.18}$$

Finally, we can solve for the optimal maximum right side probability of having the position error exceed the protection level by inserting the values $x_{j,opt}$ into (A.3):

$$P_{PE>PL+,opt} = \text{normcdf}\left(-\left[K_{MOPS}\sqrt{\sum_{i=1}^{N} x_{i,opt}^2\alpha_i^2} - \sum_{i=1}^{N} x_{i,opt}\gamma_i\right]\right) \tag{A.19}$$

The left side probability can at most be equal to this value as it is evaluating the Gaussian tail farther from the biases. We can also determine another upper bound on the left tail. It would be at its largest if all of the bias values were zero. Evaluating (7) in this case provides

$$P_{PE>PL-} \le \text{normcdf}\left(-\alpha_{\min} \times K_{V,PA}\right) \tag{A.20}$$

Therefore the left tail probability can be considered the minimum value between (A.19) and (A.20). Therefore the combined left and right tail probability can be obtained from

$$P_{PE>PL,opt} \le P_{PE>PL+,opt} + \min\left(P_{PE>PL+,opt}, P_{PE>PL-}\right) \tag{A.21}$$

This represents an upper bound on the total probability of the position error exceeding the protection level.

If all of the α values to be evaluated are identical, there is no difference in performance between the optimal calculation in (A.16) and the simplified calculation in (7). For example, if there are 14 satellites in view and all have α values of 2 and γ values of 1, both calculations return the value of $P = 2.28 \times 10^{-12}$ for a K_{MOPS} value of 5.33. However, if half of the α values are increased to 3, the simplified solution returns the same value because it uses the minimum α. However, the optimal solution returns a probability of $P = 3.25 \times 10^{-15}$, a significant improvement.